entropy

MDPI

Article

A Chain, a Bath, a Sink, and a Wall

Stefano Iubini [1,2,*], Stefano Lepri [2,3], Roberto Livi [1,2,3], Gian-Luca Oppo [4] and Antonio Politi [5]

[1] Dipartimento di Fisica e Astronomia, Università di Firenze, via G. Sansone 1, I-50019 Sesto Fiorentino, Italy; livi@fi.infn.it
[2] Istituto Nazionale di Fisica Nucleare, Sezione di Firenze, via G. Sansone 1, I-50019 Sesto Fiorentino, Italy; stefano.lepri@isc.cnr.it
[3] Consiglio Nazionale delle Ricerche, Istituto dei Sistemi Complessi, via Madonna del Piano 10, I-50019 Sesto Fiorentino, Italy
[4] SUPA and Department of Physics, University of Strathclyde, Glasgow G4 0NG, UK; g.l.oppo@strath.ac.uk
[5] Institute for Complex Systems and Mathematical Biology & SUPA, University of Aberdeen, Aberdeen AB24 3UE, UK; a.politi@abdn.ac.uk
* Correspondence: stefano.iubini@unifi.it

Received: 22 June 2017; Accepted: 24 August 2017; Published: 25 August 2017

Abstract: We numerically investigate out-of-equilibrium stationary processes emerging in a Discrete Nonlinear Schrödinger chain in contact with a heat reservoir (a bath) at temperature T_L and a pure dissipator (a sink) acting on opposite edges. Long-time molecular-dynamics simulations are performed by evolving the equations of motion within a symplectic integration scheme. Mass and energy are steadily transported through the chain from the heat bath to the sink. We observe two different regimes. For small heat-bath temperatures T_L and chemical-potentials, temperature profiles across the chain display a non-monotonous shape, remain remarkably smooth and even enter the region of negative absolute temperatures. For larger temperatures T_L, the transport of energy is strongly inhibited by the spontaneous emergence of discrete breathers, which act as a thermal wall. A strongly intermittent energy flux is also observed, due to the irregular birth and death of breathers. The corresponding statistics exhibit the typical signature of rare events of processes with large deviations. In particular, the breather lifetime is found to be ruled by a stretched-exponential law.

Keywords: discrete nonlinear schrödinger; discrete breathers; negative temperatures; open systems

PACS: 05.60.-k; 05.70.Ln; 63.20.Pw

1. Introduction

The study of nonequilibrium thermodynamics of systems composed of a relatively small number of particles is motivated by the need for a deeper theoretical understanding of the statistical laws leading to the possibility of manipulating small-scale systems like biomolecules, colloids, or nano-devices. In this framework, statistical fluctuations and size effects play a major role and cannot be ignored as it is customary to do in their macroscopic counterparts.

Arrays of coupled classical oscillators are representative models of such systems and have been studied intensively in this context [1–3]. In particular, the Discrete Nonlinear Schrödinger (DNLS) equation has been widely investigated in various domains of physics as a prototype model for the propagation of nonlinear excitations [4–6]. In fact, it provides an effective description of electronic transport in biomolecules [7] as well as of nonlinear waves propagation in layered photonic or phononic systems [8,9]. More recently, a renewed interest for this multi-purpose equation emerged in the physics of gases of ultra-cold atoms trapped in optical lattices (e.g., see [10] and references therein for a recent survey).

The DNLS dynamics are characterized by two conserved quantities: the energy density h and the mass density a (also termed norm—see the following section for their definitions). Therefore, a generic thermodynamic state of the DNLS equation can be seen as a point in the (a, h) plane. The equilibrium thermodynamics of the DNLS model was studied in a seminal paper by Rasmussen et al. [11] within the grand-canonical formalism. Here, it was shown that an equation of state can be formally derived with the help of transfer–integral techniques. Accordingly, any thermodynamic equilibrium state (a, h) can be equivalently represented in terms of a temperature T and a chemical potential μ which can be numerically determined by implementing suitable microcanonical definitions [12,13]. In Reference [11], it was found that a line of infinite–temperature equilibrium states in the (a, h) plane separates standard thermodynamic states, characterized by a positive T, from those characterized by negative absolute temperatures. The existence of negative temperatures can be traced back to the properties of the two conserved quantities of the system. From the point of view of dynamics, it was realized that negative temperatures can be associated to the presence of intrinsically localized excitations, named discrete breathers (DB) (see e.g., [14–16]). In a series of important papers, Rumpf developed entropy-based arguments to describe the asymptotic states above this infinite-temperature line [17–20]. It has been later found that negative–temperature states can form spontaneously via the dynamics of the DNLS equation. They persist over extremely long time scales, that might grow exponentially with system size as a result of an effective mechanism of ergodicity–breaking [21].

A related question is whether the dynamics of the system influences non-equilibrium properties when the system exchanges energy and/or mass with the environment. In a series of papers [21–23], it has been found that when pure dissipators act at both edges of a DNLS chain (a case sometimes called boundary cooling [24–27]) the typical final state consists of an isolated static breather embedded in an almost empty background. The breather collects a sensible fraction of the initial energy and it is essentially decoupled from the rest of the chain. The spontaneous creation of localized energy spots out of fluctuations has further consequences on the relaxation to equipartition, since the interaction with the remaining part of the chain can become exponentially weak [28,29]. A similar phenomenon occurs after a quench from high to low temperatures in oscillator lattices [30]. Also, boundary driving by external forces may induce non-linear localization [31–33].

When, instead, the chain is put in contact with thermal baths at its edges, non-equilibrium stationary states characterized by a gradient of temperature and chemical potential emerge [13]. Local equilibrium is typically satisfied so that the overall state of the chain can be conveniently represented as a path in the (a, h) plane connecting two points corresponding to the thermodynamic variables imposed by the two reservoirs. The associated transport of mass and energy is typically normal (diffusive) and can be described in terms of the Onsager formalism. However, peculiar features, such as non-monotonous temperature profiles [34] or persistent currents [35], are found as well as a signature of anomalous transport in the low-temperature regime [36,37].

In this paper we consider a set-up where one edge is in contact with a heat reservoir at temperature T_L and chemical potential μ_L, while the other interacts with a pure dissipator, i.e., a mass sink. The original motivation for studying this configuration was to better understand the role of DBs in thermodynamic conditions. At variance with standard set-ups [1,2], this is conceptually closer to a semi-infinite array in contact with a single reservoir. In fact, on the pure-dissipator side, mass can only flow out of the system.

The presence of a pure dissipator forces the corresponding path to terminate close to the point $(a = 0, h = 0)$, which is singular both in T and μ. This is indeed the point where the infinite- and the zero-temperature lines collapse. Therefore, slight deviations may easily lead to crossing the $\beta = 0$ line, where $\beta = 1/T$ is the inverse temperature. This is indeed the typical scenario observed for small T_L, when β smoothly changes sign twice before approaching the dissipator (see Figure 1 for a few sampled paths). The size of the negative-temperature region increases with T_L and appears to be stable over long time scales. Upon further increasing T_L, a different stationary regime is found, characterized by strong fluctuations of mass and energy flux. In practice, the negative-temperature region first

extends up to the dissipator edge and then it progressively shrinks in favour of a positive-temperature region (on the other side of the chain). In this regime, the dynamics are controlled by the spontaneous formation (birth) and disappearance (death) of discrete breathers.

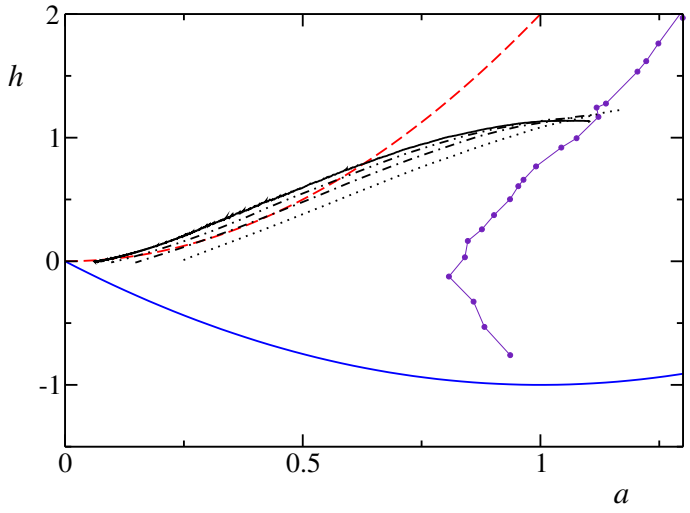

Figure 1. Phase diagram of the DNLS equation in the $(a-h)$ plane of, respectively, energy and mass densities. The positive-temperature region extends between the ground state $\beta = +\infty$ line (solid blue lower curve) and the $\beta = 0$ isothermal (red dashed curve). Purple circles show the $\mu = 0$ line, which has been determined numerically through equilibrium simulations (data are taken from Reference [13]). Black curves refer to nonequilibrium profiles obtained by employing a heat bath with parameters $T_L = 3$ and $\mu_L = 0$ and a pure dissipator located at the left and right edges of the chain, respectively. Dotted, dot-dashed, dot-dot-dashed and solid curves refer to chain sizes $N = 511$, 1023, 2047, and 4095, respectively. Upon increasing N, these above profiles tend to enter the negative temperature region. Simulations are performed by evolving the DNLS chain over 10^7 time units after a transient of 4×10^7 units. For the system size $N = 4095$, a further average over 10 independent trajectories is performed.

In Section 2 we introduce the model and briefly recall the definition of the main observables. Section 3 is devoted to a detailed characterization of the low-temperature phase, while the far-from-equilibrium phase observed for large T_L is discussed in Section 4. This is followed by the analysis of the statistical properties of the birth/death process of large-amplitude DBs, illustrated in Section 5. Finally, in Section 6 we summarize the main results and comment about possible relationships with similar phenomena previously reported in the literature.

2. Model and Methods

We consider a DNLS chain of size N and with open boundary conditions, whose bulk dynamics is ruled by the equation

$$i\dot{z}_n = -2|z_n|^2 z_n - z_{n-1} - z_{n+1} \tag{1}$$

where $(n = 1, \ldots, N)$ and $z_n = (p_n + iq_n)/\sqrt{2}$ are complex variables, with q_n and p_n being standard conjugate canonical variables. The quantity $a_n = |z_n(t)|^2$ can be interpreted as the *number of particles*, or, equivalently, the *mass* in the lattice site n at time t. Upon identifying the set of canonical variables z_n and iz_n^*, Equation (1) can be read as the equation of motion generated by the Hamiltonian functional

$$H = \sum_{n=1}^{N} \left(|z_n|^4 + z_n^* z_{n+1} + z_n z_{n+1}^* \right) \tag{2}$$

through the Hamilton equations $\dot{z}_n = -\partial H/\partial(iz_n^*)$. We are dealing with a dimensionless version of the DNLS equation: the nonlinear coupling constant and the hopping parameters, which are usually indicated explicitly in the Hamiltonian (2), have been set equal to unity. Accordingly, also the time variable t is expressed in arbitrary adimensional units. Without loss of generality, this formulation has the advantage of simplifying numerical simulations.

A relevant property of the DNLS dynamics is the existence of a second conserved quantity beside the total energy H, namely the total mass

$$A = \sum_{n=1}^{N} |z_n|^2 \,. \tag{3}$$

As a result, an equilibrium state is specified by two parameters, the mass density $a = A/N \geq 0$ and the energy density $h = H/N$. The first reconstruction of the equilibrium phase-diagram (a, h) of the DNLS equation was reported in [11]. It is reproduced in Figure 1 for our choice of parameters, where the lower solid line defines the $(T = 0)$ ground-state line $h = a^2 - 2a$ for different values of the mass density a. The ground-state corresponds to a uniform state with constant amplitude and constant phase-differences $z_n = \sqrt{a}e^{i(\mu t + \pi n)}$, with $\mu = 2(a - 1)$. States below this curve are not physically accessible. The positive-temperature region lies above the ground-state up to the red dashed line $h = 2a^2$, which corresponds to the infinite-temperature $(\beta = 0)$ line. In this limit, the grand-canonical equilibrium distribution becomes proportional to $\exp(\beta\mu A)$, where the finite (negative) product $\beta\mu$ implies a diverging chemical potential. Equilibrium states at infinite temperature are therefore characterized by an exponential distribution of the amplitudes $P(|z_n|^2) = a^{-1}e^{-|z_n|^2/a}$ and random phases. Finally, states above the $\beta = 0$ line belong to the so-called negative-temperature region [11,21].

Finite-temperature equilibrium states do not allow for straightforward analytical treatments. However, one can determine the relation $a(T, \mu)$, $h(T, \mu)$ numerically, by putting the system in interaction with an external reservoir (see below) that imposes T and μ and by measuring the corresponding equilibrium densities. This method was adopted in Reference [13] to identify the $\mu = 0$ line shown in Figure 1. Upon increasing μ, the curve moves to the right in the (a, h) diagram and becomes more and more vertical (data not shown). Isothermal lines $T = c$ can be found analogously: they roughly follow the profile of the $T = 0$ line and, upon increasing c, they span all the positive-temperature region, approaching the infinite-temperature line for $c \to +\infty$ [13].

A non-equilibrium steady state can be represented as a path in the (a, h)-parameter space, where $a(x)$ is the mass density, $h(x)$ the energy density, and $x = n/N$ the rescaled position along the chain. In our set-up, the first site of the chain $(n = 1)$ is in contact with a reservoir at temperature T_L and chemical potential μ_L. This is ensured by implementing the non-conservative Monte-Carlo dynamics described in Reference [13]. In a few words, the reservoir performs random perturbations $\delta z_1 = (\delta p_1 + i\delta q_1)/\sqrt{2}$ of the state variable z_1 that are accepted or rejected according to a grand-canonical Metropolis cost-function $\exp[-T_L(\Delta H - \mu_L \Delta A)]$, where ΔH and ΔA are respectively the variations of energy and mass produced by δz_1. The perturbations δp_1 and δq_1 are independent random variables extracted from a uniform distribution in the interval $[-R, R]$. The opposite site $(n = N)$ interacts with a pure *stochastic dissipator* that sets the variable z_N equal to zero, thus absorbing an amount of mass equal to $|z_N|^2$. Both the heat bath and the dissipator are activated at random times, whose separations are independent and identically distributed variables uniformly distributed within the interval $[t_{min}, t_{max}]$. On average, this corresponds to simulating an interaction process with decay rate $\gamma \sim \bar{t}^{-1}$, where $\bar{t} = (t_{max} + t_{min})/2$. Notice that different prescriptions, such as for example a Poissonian distribution of times with average $\bar{t}$ or a constant pace equal to $\bar{t}$, do not introduce any relevant modification in the dynamical and statistical properties of the model (1). Finally, the Hamiltonian dynamics between successive interactions with the environment has been generated by implementing a symplectic, 4th-order Yoshida algorithm [38]. We have verified that a time step $\Delta t = 2 \times 10^{-2}$ suffices to ensure suitable accuracy.

Throughout the paper we deal with measurements of temperature profiles. Since the DNLS Hamiltonian is not separable, the standard relation between temperature and local kinetic energy does not hold. Due to the existence of the second conserved quantity A, it is necessary to make use of the microcanonical definition provided in [39] and further extended in [12]. Its derivation is founded on the thermodynamic relation

$$\beta = T^{-1} = \left.\frac{\partial S}{\partial E}\right|_{A=M} \tag{4}$$

for a system with total energy $H = E$, total mass $A = M$ and entropy S. The calculation amounts to derive a measure of the hyper-surface at constant energy and mass in the phase space and to compute its variation with respect to E at constant mass. The general expression of T is a thermal average of a non-local function of the dynamical variables z_n and z_n^* and is rather involved; we refer to [13,21] and the related bibliography for theoretical and computational details.

In what follows, we consider a situation where all parameters, other than T_L, are kept fixed. In particular, we have chosen $\mu_L = 0$, $R = 0.8$ and $\bar{t} = 3 \times 10^{-2}$, with t_{max} and t_{min} of order 10^{-2}. We have verified that the results obtained for this choice of the parameter values are general. A more detailed account of the dependence of the results on the thermostat properties will be reported elsewhere.

Finally, we recall the observables that are typically used to characterize a steady-state out of equilibrium: the mass flux

$$j_a = 2\langle \mathrm{Im}(z_n^* z_{n+1}) \rangle \,, \tag{5}$$

and the energy flux

$$j_h = 2\langle \mathrm{Re}(\dot{z}_n z_{n+1}^*) \rangle \,, \tag{6}$$

where the angular brackets denote a time average.

3. Low-Temperature Regime: Coupled Transport and Negative Temperatures

In the left panel of Figure 2, we report the average profile of the inverse temperature $\beta(x)$ as a function of the rescaled site position $x = n/N$, for different values of the temperature of the thermostat. A first "anomaly" is already noticeable for relatively small T_L: the profile is non monotonous (see for example the curve for $T_L = 1$). This feature is frequently encountered when a second quantity, besides energy, is transported [13,40,41]. In the present setup, this second thermodynamic observable is the chemical potential $\mu(x)$, set equal to zero at the left edge. Rather than plotting $\mu(x)$, in the right panel of Figure 2, we have preferred to plot the more intuitive mass density $a(x)$. There we see that the profile for $T_L = 1$ deviates substantially from a straight line, indicating that the thermodynamic properties vary significantly along the chain and suggesting that the lattice might not be long enough to ensure an asymptotic behavior.

To clarify this point, we have performed simulations for different values of N. The results for $T_L = 1$ are reported in Figure 3, where we plot the local temperature T as a function of x. All profiles start from $T = 1$, the value imposed by the thermostat and, after an intermediate bump, eventually attain very small values. Since neither the temperature nor the chemical potential are directly imposed by the purely dissipating "thermostat", it is not obvious to predict the asymptotic value of the temperature (and the chemical potential). The data reported in the inset suggest a sort of logarithmic growth with N, but this is not entirely consistent with the results obtained for $T_L = 3$ (see below).

If transport were normal and N were large enough, the various profiles should collapse onto each other, but this is far from the case displayed in Figure 3. The main reason for the lack of convergence is the growth of the temperature bump. This is because, upon further increases of N, the system spontaneously crosses the infinite temperature line and enters the negative-temperature region. For $T_L = 3$, this "transition" has already occurred for $N = 4095$, as it can be seen in Figure 2. The crossings of the infinite temperature points ($\beta = 0$) at the boundaries of the negative temperature region correspond to infinite (negative) values of the chemical potential μ in such a way that the

product $\beta\mu$ remains finite at these turning points (data not reported). To our knowledge, this is the first example of negative-temperature states robustly obtained and maintained in nonequilibrium conditions in a chain coupled with a single reservoir at positive temperature. In order to shed light on the thermodynamic limit, we have performed further simulations for different system sizes. In Figure 4, we report the results obtained for $T_L = 3$ and N ranging from 511 to 4095. In Figure 4a, we see that the negative-temperature region is already entered for $N = 1023$. Furthermore, its extension grows with N, suggesting that in the thermodynamic limit it would cover the entire profile but the edges.

Since non-extensive stationary profiles have been previously observed both in a DNLS and a rotor chain (i.e., the XY-model in $d = 1$) at zero temperature and in the presence of chemical potential gradients [42], it is tempting to test to what extent an anomalous scaling (say $n/\sqrt{N}$) can account for the observations. In the inset of Figure 4a, we have rescaled the position along the lattice by $\sqrt{N}$. For relatively small but increasing values of $n/\sqrt{N}$ we do see a convergence towards an asymptotic curve, which smoothly crosses the $\beta = 0$ line. This suggests that close to the left edge, positive temperatures extend over a range of order $\mathcal{O}(\sqrt{N})$, thereby covering a non-extensive fraction of the chain length. The scaling behavior in the rest of the chain is less clear, but it is possibly a standard extensive dynamics characterized by a finite temperature on the right edge. A confirmation of the anomalous scaling in the left part of the chain is obtained by plotting the profiles of h and a again as a function of $n/\sqrt{N}$ (see the panels (b) and(c) in Figure 4, respectively). Further information can be extracted from the scaling behavior of the stationary mass flux j_a. In Figure 5, we report the average value of j_a as a function of the lattice length. There, we see that j_a decreases roughly as $N^{-1/2}$. At a first glance this might be interpreted as a signature of energy super-diffusion, but it is more likely due to the presence of a pure dissipation on the right edge (in analogy to what seen in the XY-model [43]).

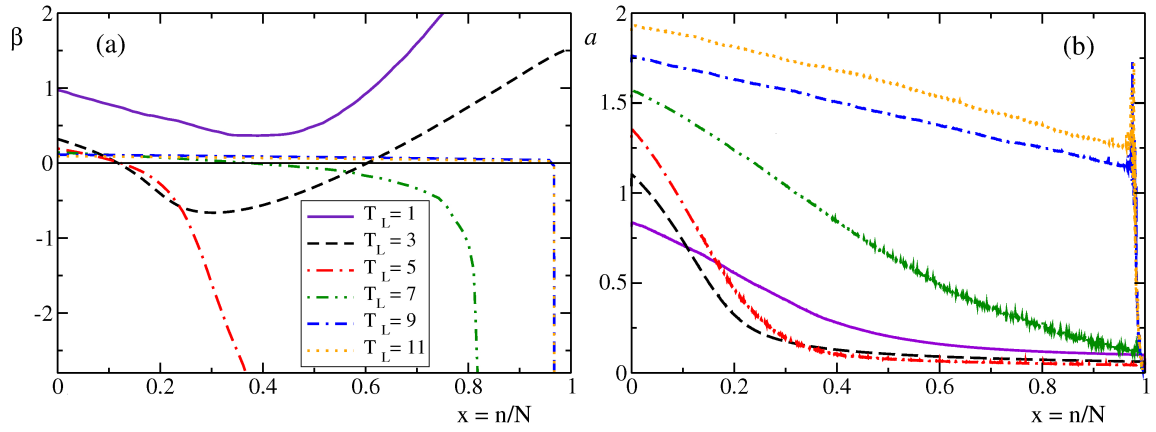

Figure 2. Average profiles of the inverse temperature $\beta(x)$ (panel (**a**)) and mass-density $a(x)$ (panel (**b**)) for a DNLS chain with $N = 4095$ and different temperatures T_L of the reservoir acting at the left edge, where $\mu = 0$. The profile $\beta(x)$ is computed making use of the microcanonical definition of temperature. Simulations are performed evolving the DNLS chain over 10^7 time units after a transient of 4×10^7 units. In order to obtain a reasonable smoothing of these time-averaged profiles we have further averaged each of them over 10 independent trajectories.

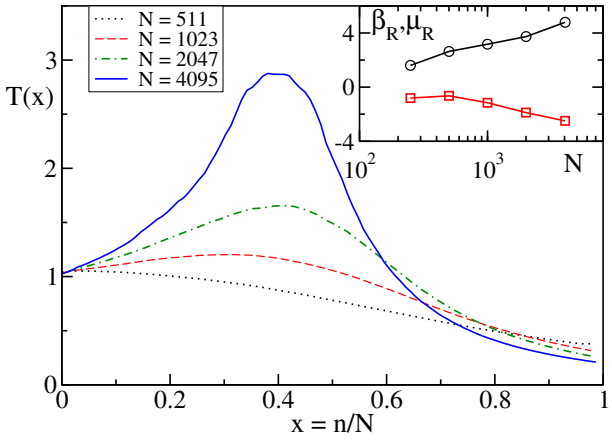

Figure 3. Average profiles of the temperature $T(x)$ for $T_L = 1$ and different system sizes N. The profile $T(x)$ is computed by means of the microcanonical definition of temperature. The inset shows the boundary inverse temperature β_R (black circles) and chemical potential μ_R (red squares) close to the dissipator side as a function of the system size N. The data refers to the microcanonical definitions of temperature and chemical potential computed on the last 10 sites of the chain. Simulations are performed evolving the system over 10^7 time units after a transient of 4×10^7 units. For the system size $N = 4095$ a further average over 10 independent trajectories has been performed.

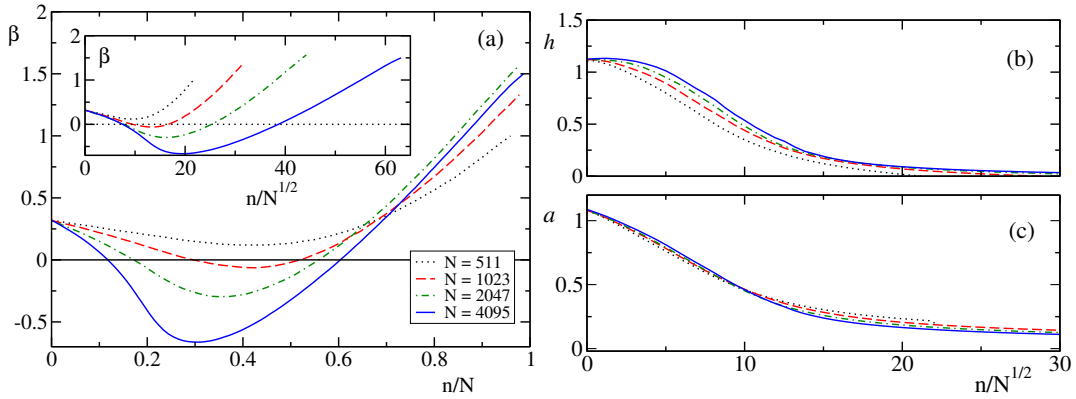

Figure 4. Panel (**a**): average profiles of inverse temperature β for $T_L = 3$ and different system sizes N. The profile β is computed by means of the microcanonical definition of temperature. In the inset, an alternative scaling by $1/\sqrt{N}$ is proposed. For the same setup, panels (**b**,**c**) show the behavior of the energy profile h and the mass profile a, respectively (again scaling the position by $\sqrt{N}$). Simulations are performed evolving the DNLS chain over 10^7 time units after a transient of 4×10^7 units. For the system size $N = 4095$, a further average over ten independent trajectories is performed.

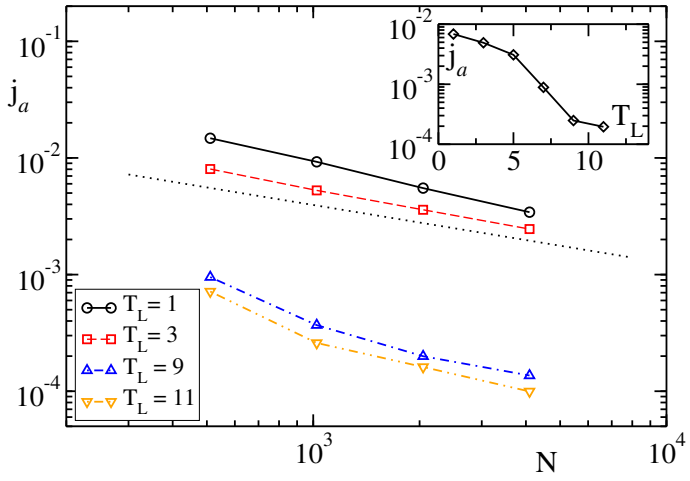

Figure 5. Average mass flux j_a versus system size N for different reservoir temperatures T_L. The black dotted line refers to a power-law decay $j_a \sim N^{-1/2}$. The inset shows the dependence of j_a on the reservoir temperature T_L for the system size $N = 4095$. Simulations are performed evolving the DNLS chain over 10^7 time units after a transient of 4×10^7 units. For the system size $N = 4095$ we have averaged over 10 independent trajectories.

In stationary conditions, mass, and energy fluxes are constant along the chain. This is not necessarily true for the heat flux, as it refers only to the incoherent component of the energy transported across the chain. More precisely, the heat flux is defined as $j_q(x) = j_h - j_a \mu(x)$ [43] Since j_a and j_h are constant, the profile of the heat flux j_q is essentially the same of the μ profile (up to a linear transformation). In Figure 6a, we report the heat flux for $T_L = 1$. It is similar to the temperature profile displayed in Figure 3. It is not a surprise to discover that j_q is larger where the temperature is higher. Figure 6b in the same Figure 6 refers to $T_L = 3$. A very strange shape is found: the flux does not only changes sign twice but exhibits a singular behavior in correspondence of the change of sign, as if a sink and source of heat were present in these two points, where the chemical potential and the local temperature diverge (see, e.g., the red dashed line in Figure 6b representing the β profile). The scenario looks less awkward if the entropy flux $j_s = j_q/T$ is monitored. For $T_L = 1$, the bump disappears and we are in the presence of a more "natural" shape (see Figure 6d) More important is to note that the singularities displayed by j_q for $T_L = 3$ are almost removed since they occur where $T \to \infty$ (we are convinced that the residual peaks are due to a non perfect identification of the singularities). If one removed the singular points, the profile of the entropy flux $j_s = j_q/T$ has a similar shape for the cases $T_L = 1$ and $T_L = 3$. A more detailed analysis of the scenario is, however, necessary in order to provide a solid physical interpretation.

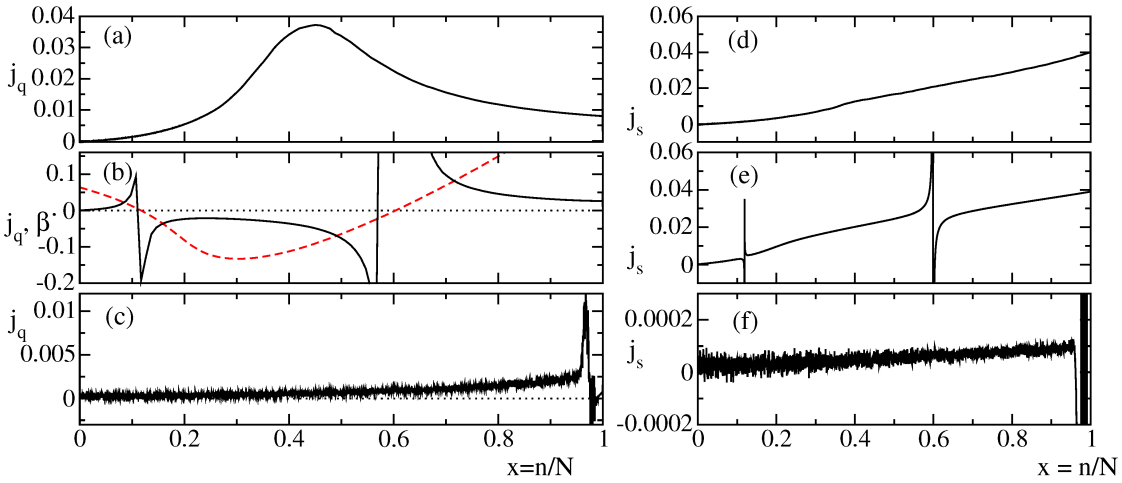

Figure 6. Profiles of heat flux (black lines) for $T_L = 1$ (panel (**a**)), $T_L = 3$ (panel (**b**)) and $T_L = 9$ (panel (**c**)) in a chain with $N = 4095$ lattice sites. For each boundary temperature, we find the following values of mass and energy fluxes: panel (**a**) $j_a = 3.5 \times 10^{-3}$, $j_h = -3.3 \times 10^{-4}$; panel (**b**) $j_a = 2.5 \times 10^{-3}$, $j_h = 3.4 \times 10^{-4}$; panel (**c**) $j_a = 1.2 \times 10^{-4}$, $j_h = 1.5 \times 10^{-4}$. The red dashed line in panel (**b**) refers to the rescaled profile of the inverse temperature $\beta'(x) = \beta(x)/5$ measured along the chain (see Figure 2). Panels (**d**–**f**) show the profiles of entropy flux for the same temperatures: $T_L = 1$, $T_L = 3$ and $T_L = 9$, respectively. Other simulation details are the same as given in Figure 2.

4. High Temperature Regime: DB Dominated Transport

Let us now turn our attention to the high-temperature case. As shown in Figure 2a, for sufficiently large T_L values, the positive-temperature region close to the dissipator disappears (this is already true for $T_L = 5$) and, at the same time, the positive-temperature region on the left grows. In other words, negative temperatures are eventually restricted to a tiny region close to the dissipator side. This stationary state is induced by the spontaneous formation and the destruction of large DBs close to the dissipator. On average, such a process gives rise to locally steep amplitude profiles that are reminiscent of barriers raised close to the right edge of the chain, see Figure 2b. As it is well known, DBs are localized nonlinear excitations typical of the DNLS chain. Their phenomenology has been widely described in a series of papers where it has been shown that they emerge when energy is dissipated from the boundaries of a DNLS chain [21–23]. In fact, when pure dissipators act at both chain boundaries, the final state turns out to be an isolated DB embedded in an almost empty background. In view of its localized structure and the fast rotation, the DB is essentially uncoupled from the rest of the chain and, a fortiori, from the dissipators. One cannot exclude that a large fluctuation might eventually destroy the DB, but this would be an extremely rare event.

In the setup considered in this paper, DB formation is observed in spite of one of the two dissipators being replaced by a reservoir at finite temperature. DBs are spontaneously produced close to the dissipator edge only for sufficiently high values of T_L. Due to its intrinsic nonlinear character, this phenomenon cannot be described in terms of standard linear-response arguments. In particular, the temperature reported in the various figures cannot be interpreted as the temperature of specific local-equilibrium state: it is at best the average over the many different macrostates visited during the simulation. Actually, it is even possible for some of theses macrostates to deviate substantially from equilibrium. Therefore, we limit ourselves to some phenomenological remarks. The spontaneous formation of small breathers close to the right edge drastically reduces the dissipation and contributed to a further concentration of energy through the merging of the DBs into fewer larger ones and, eventually, to a single DB. Mechanisms of DB-merging have already been encountered under different conditions in the DNLS model [21]. The onset of a DB essentially decouples the left from the right regions of the chain. In particular, it strongly reduces the energy and mass currents fluxes. One can

spot DBs simply by looking at the average mass profiles. In Figure 2, the presence of a DB is signaled by the sharp peak close to the right edge for both $T_L = 9$ and $T_L = 11$.

The region between the reservoir and the DB should, in principle, evolve towards an equilibrium state at temperature T_L. However, a close look at the β-profile in Figure 2 reveals the presence of a moderate temperature gradient that is typical of a stationary non-equilibrium state. In fact, DBs are not only born out of fluctuations, but can also collapse due to local energy fluctuations. As shown in Figure 7a, once a DB is formed, it tends to propagate towards the heat reservoir located at the opposite edge. The DB position is tagged by black dots drawn at fixed time intervals over a very long time lapse of $\mathcal{O}(10^6)$, in natural time units of the model. This backward drift comes to a "sudden" end when a suitable energy fluctuation destroys the DB (see Figure 7a). Afterwards, mass and energy start flowing again towards the dissipator, until a new DB is spontaneously formed by a sufficiently large fluctuation close to the dissipator edge (the formation of the DB is signaled by the rightmost black dots in Figure 7a) and the conduction of mass and energy is inhibited again. The DB lifetime is rather stochastic, thus yielding a highly irregular evolution. The statistical properties of such birth/death process are discussed in the following section.

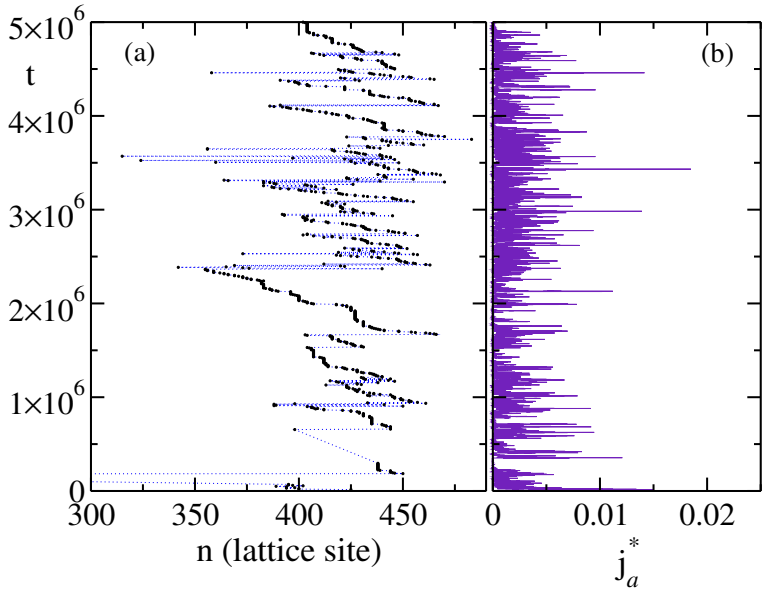

Figure 7. (**a**) Qualitative DB trajectory in a stationary state with $N = 511$ and $T_L = 10$. Each point of the curve corresponds to the position of the maximum average amplitude of the chain in a temporal window of 5×10^3 time units. (**b**) Temporal evolution of the outgoing mass flux j_a^* through the dissipator edge during the same dynamics of panel (a). The flux j_a^* is computed every 20 time units as the average amount of mass flowing to the dissipator during such time interval. Higher peaks typically correspond to the breakdown of one or more DBs. Notice that the boundary mass flux can take only positive values because the chain interacts with a pure dissipator.

The statistical process describing the appearance/disappearance of the DB is a complex one. On the one hand, we are in the presence of a stationary regime: the mass and energy currents flowing through the dissipator are found to be constant, when averaged over time intervals much longer than the typical DB lifetime. On the other hand, strong fluctuations in the DB lifetime mean that this regime is not steady but it rather corresponds to a sequence of many different macrostates, some of which are likely to be far from equilibrium. Altogether, in this phase, the presence of long lasting DBs induces a substantial decrease of heat and mass conduction. This is clearly seen in Figure 5, where j_a is plotted for different chain lengths. The two set of data corresponding to $T_L = 9$ and 11 are at least one order of magnitude below those obtained in the low-temperature phase. The sharp crossover that separates the

two conduction regimes is neatly highlighted in the inset of Figure 5, where the stationary mass flux is reported as a function of the reservoir temperature for the size $N = 4095$.

The effect of the appearance and disappearance of the DB in the high reservoir temperature regime on the transport of heat and mass along the chain is twofold. During the fast dynamics, it produces bursts in the output fluxes of these quantities as demonstrated in Figure 7b. When the DB is present the boundary flux to the dissipator decreases, while when the DB disappears, avalanches of heat and mass reach the dissipator. In the slow dynamics obtained by averaging over many bursts, the conduction of heat and mass from the heat reservoir to the dissipator is hugely reduced with respect to the low temperature regime. We can conclude that the most important effect of the intermittent DB in the high temperature regime is to act as a thermal wall.

Finally, in Figure 6c,f we plot the heat and entropy profiles observed in the high-temperature phase, respectively. The strong fluctuations in the profiles are a consequence of the large fluctuations in the DB birth/death events and its motion. It is now necessary to average over much longer time scales to obtain sufficiently smooth profiles. It is interesting, however, to observe that the profile of j_s in Figure 6f exhibits an overall shape similar to that observed in the low temperature regimes (see Figure 6d,e). This notwithstanding, there are two main differences with the low temperature behavior. First, close to the right edge of the dissipator we are now in presence of wild fluctuations of j_s, and second the overall scale of the entropy flux profile is heavily reduced.

5. Statistical Analysis

In order to gain information on the high-temperature regime, it is convenient to look at the fluctuations of the boundary mass flux j_a^* and the boundary energy flux j_h^* flowing through the dissipator edge. In Figure 8 we plot the distribution of both j_a^* (panel (a)) and j_h^* (panel (b)) for $T_L = 11$ for different chain lengths. In both cases, power-law tails almost independent of N are clearly visible. This scenario is highly reminiscent of the avalanches occurring in sandpile models. In fact, one such analogy has been previously invoked in the context of DNLS dynamics to characterize the atom leakage from dissipative optical lattices [44].

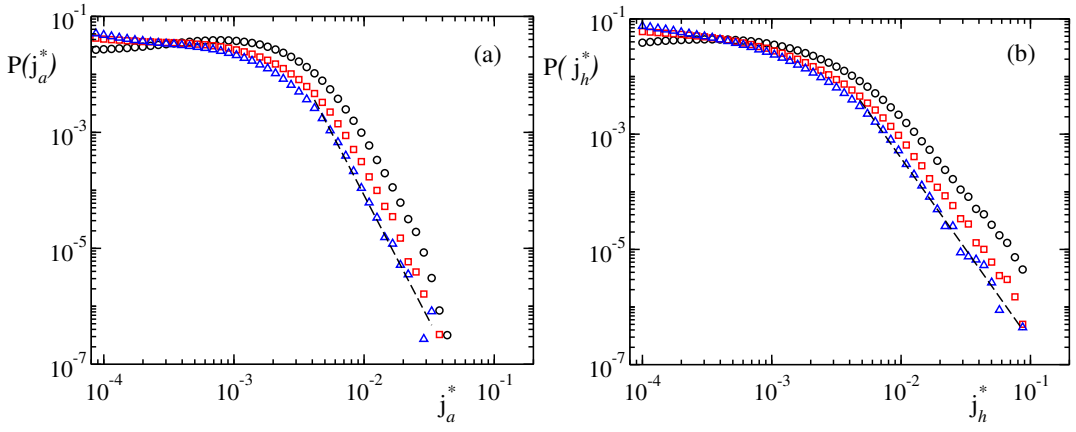

Figure 8. Normalized boundary flux distributions through the dissipator for a stationary state with $T_L = 11$. Panel (**a**) shows the mass flux distribution $P\left(j_a^*\right)$, while panel (**b**) refers to the energy flux distribution $P\left(j_h^*\right)$. Black circles, red squares, and blue triangles refer to system sizes $N = 511, 1023$, and 2047, respectively. Power-law fits on the largest size $N = 2047$ (see black dashed lines) give $P(j_a^*) \sim j_a^{*-4.32}$ and $P(j_h^*) \sim j_h^{*-3.17}$. Boundary fluxes are sampled by evolving the DNLS chain for a total time t_f after a transient of 4×10^7 temporal units and averaged over time windows of five temporal units. For the sizes $N = 511$ and $N = 1023$ we have considered a single trajectory with $t_f = 10^8$. For the size $N = 2047$ the distributions are extracted from five independent trajectories with $t_f = 2 \times 10^7$.

We processed the time series of the type reported in Figure 7b to determine the duration τ_b of the bursts (avalanches) and τ_l of the "laminar" periods in between consecutive bursts (i.e., the DB life-times). In practice, we have first fixed a flux threshold ($s = 4.25 \times 10^{-3}$) to distinguish between burst and laminar periods. Furthermore, a series of bursts separated by a time shorter than $dt_0 = 10^3$ has been treated as a single burst. This algorithm has been applied to 20 independent realizations of the DNLS dynamics in the high-temperature regime. Each realization has been obtained by simulating a lattice with $N = 511$ sites, $T_L = 10$, and for a total integration time $t = 5 \times 10^6$. In these conditions we have recorded nearly 7000 avalanches.

The probability distribution of the burst duration is plotted in Figure 9a. It follows a a Poissonian distribution, typical of random uncorrelated events. We have also calculated the amount of mass A and energy E associated with each burst, integrating mass, and energy fluxes during each burst. The results are shown as a scatter plot in the inset of Figure 9a. They display a clear (and unsurprising) correlation between these two quantities.

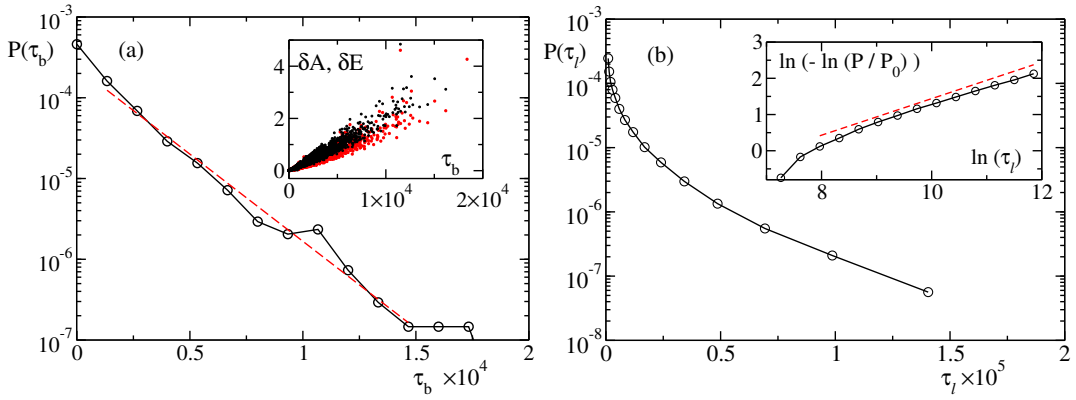

Figure 9. (**a**) Probability distribution of the duration of bursts τ_b. Note the logarithmic scale on the vertical axis. From an exponential fit $P \sim \mathrm{e}^{-\gamma\tau_b}$, we find a decay constant $\gamma = 5 \times 10^{-4}$ (red dashed line). The inset shows the relation between the duration τ_b and the amount of mass δA (black dots) and energy δE (red dots) released to the dissipator. (**b**) Probability distribution of DB lifetimes. In the inset we show that this is compatible with a stretched exponential law $P = P_0 \mathrm{e}^{-\tau_l^\sigma}$, where $\sigma \simeq 0.5$ (red dashed line) and P_0 is the maximum value of the distribution.

The time interval between two consecutive bursts is characterized by a small mass flux. Typically, during this period the chain develops a stable DB that inhibits the transfer of mass towards the dissipator. Figure 9b shows the probability distribution of the duration of these laminar periods. The distribution displays a stretched-exponential decay with a characteristic constant $\sigma = 0.5$. Such a scenario is consistent with the results obtained in [26] for the Fermi-Pasta-Ulam chain and in [22] for the DNLS lattice. The values of the power σ found in these papers are not far from the one that we have obtained here (see also [45] for similar results on rotor models).

Altogether, there is a clear indication that the statistics of the duration of avalanches and walls is controlled by substantially different mechanisms. It seems that the death of a wall/DB is ruled by rare event statistics [22,26,45], while its birth appears as a standard activation process emerging when an energy barrier is eventually overtaken. In fact, when mass starts flowing through the dissipator edge after the last death of a wall/DB, we have to wait for the spontaneous *activation* of a new wall/DB before the mass flux vanishes again. Conversely, the wall/DB is typically found to persist over much longer time scales and its eventual destruction is determined by a very rare fluctuation, whose amplitude is expected to be sufficiently large to compete with the energy that, in the meanwhile, has been collected by the wall/DB during its motion towards the reservoir.

6. Conclusions

We have investigated the behavior of a discrete nonlinear Schrödinger equation sandwiched between a heat reservoir and a mass/energy dissipator. Two different regimes have been identified upon changing the temperature T_L of the heat reservoir, while keeping fixed the properties of the dissipator. For low T_L and low chemical potential, a smooth β-profile is observed, which extends (in the central part) to negative temperatures without, however, being accompanied by the formation of discrete breathers over the time scales accessible to numerical simulations. In the light of the theoretical achievements by Rumpf [17–20], the negative-temperature regions are incompatible with the assumption of local thermodynamic equilibrium, which instead appears to be satisfied in the positive-temperature part. Therefore, despite the smoothness of the profiles and the stationarity of mass and energy fluxes, such negative-temperature configurations should be better considered as metastable states. Unfortunately, it is not easy to investigate this regime; no single heat bath can impose a fixed negative T in a meaningful way so as to be able to compare with equilibrium states. It is therefore necessary to simulate larger systems in the hope to observe the spontaneous formation of breathers, the only obvious signature of negative temperatures. We plan to undertake such a kind of numerical studies in the near future. It is nevertheless remarkable to see that negative temperatures are steadily sustained for moderately long chain lengths. As a second anomaly, we report the slow decrease of the mass-flux with the chain length: the hallmark of an unconventional type of transport. This feature is, however, not entirely new; a similar scenario has been previously observed in setups with dissipative boundary conditions and no fluctuations [42].

For larger temperatures T_L, we observe an intermittent regime characterized by the alternation of insulating and conducting states, triggered by the appearance/disappearance of discrete breathers. Note that this regime is rather unusual, since it is generated by increasing the amount of energy provided by the heat bath rather than by decreasing the chemical potential, as observed for example in the superfluid/Mott insulator transition in Bose-Einstein condensates in optical lattices. Although, for clarity, we referred to the low and high T_L cases, there is no special difference to be expected in the intermediate regime, except for the typical timescale for DB creation that may be, still, exceedingly large. In fact, for finite N, such a timescale becomes much shorter above some typical T_L.

The intermittent presence of a DB/wall makes the chain to behave as a *rarely leaking pipe*, which releases mass droplets at random times when the DB disappears according to a stretched-exponential distribution. The resulting fluctuations of the fluxes suggest that the regime is stationary but not steady, i.e., locally the chain irregularly oscillates among different macroscopic states characterized, at best, by different values of the thermodynamic variables. A similar scenario is encountered in the XY chain, when both reservoirs are characterized by a purely dissipation accompanied by a deterministic forcing [42]. In such a setup, as discussed in Reference [42], the temperature in the middle of the chain fluctuates over macroscopic scales. Here, however, given the rapidity of changes induced by the DB dynamics, there may be no well-defined values of the thermodynamic observables. For example, during an avalanche it is unlikely that temperature and chemical potentials are well-defined quantities, as there may not even be a local equilibrium. This extremely anomalous behavior is likely to smear out in the thermodynamic limit, since the breather life-time does not probably increase with the system size, however, it is definitely clear that the associated fluctuations strongly affect moderately-long DNLS chains.

Acknowledgments: This research did not receive any funding. Stefano Lepri acknowledges hospitality of the Institut Henri Poincaré-Centre Emile Borel during the trimester Stochastic Dynamics Out of Equilibrium where part of this work was elaborated.

Author Contributions: Stefano Iubini performed the numerical simulations. All Authors contributed to the research work and to writing the paper.

Conflicts of Interest: The authors declare no conflict of interest.

Abbreviations

The following abbreviations are used in this manuscript:

DNLS Discrete Nonlinear Schrödinger
DB Discrete Breather

References

1. Lepri, S.; Livi, R.; Politi, A. Thermal conduction in classical low-dimensional lattices. *Phys. Rep.* **2003**, *377*, 1–80.
2. Dhar, A. Heat Transport in low-dimensional systems. *Adv. Phys.* **2008**, *57*, 457–537.
3. Basile, G.; Delfini, L.; Lepri, S.; Livi, R.; Olla, S.; Politi, A. Anomalous transport and relaxation in classical one-dimensional models. *Eur. Phys J. Spec. Top.* **2007**, *151*, 85–93.
4. Eilbeck, J.C.; Lomdahl, P.S.; Scott, A.C. The discrete self-trapping equation. *Physica D* **1985**, *16*, 318–338.
5. Eilbeck, J.C.; Johansson, M. *The Discrete Nonlinear Schrödinger Equation-20 Years on*; World Scientific: Singapore, 2003.
6. Kevrekidis, P.G. *The Discrete Nonlinear Schrödinger Equation*; Springer: Berlin/Heidelberg, Germany, 2009.
7. Scott, A. *Nonlinear Science. Emergence and Dynamics of Coherent Structures*; Oxford University Press: Oxford, UK, 2003.
8. Kosevich, A.M.; Mamalui, M.A. Linear and nonlinear vibrations and waves in optical or acoustic superlattices (photonic or phonon crystals). *J. Exp. Theor. Phys.* **2002**, *95*, 777.
9. Hennig, D.; Tsironis, G. Wave transmission in nonlinear lattices. *Phys. Rep.* **1999**, *307*, 333–432.
10. Franzosi, R.; Livi, R.; Oppo, G.; Politi, A. Discrete breathers in Bose–Einstein condensates. *Nonlinearity* **2011**, *24*, R89.
11. Rasmussen, K.; Cretegny, T.; Kevrekidis, P.G.; Grønbech-Jensen, N. Statistical mechanics of a discrete nonlinear system. *Phys. Rev. Lett.* **2000**, *84*, 3740–3743.
12. Franzosi, R. Microcanonical Entropy and Dynamical Measure of Temperature for Systems with Two First Integrals. *J. Stat. Phys.* **2011**, *143*, 824–830.
13. Iubini, S.; Lepri, S.; Politi, A. Nonequilibrium discrete nonlinear Schrödinger equation. *Phys. Rev. E* **2012**, *86*, 011108.
14. Sievers, A.; Takeno, S. Intrinsic localized modes in anharmonic crystals. *Phys. Rev. Lett.* **1988**, *61*, 970.
15. MacKay, R.; Aubry, S. Proof of existence of breathers for time-reversible or Hamiltonian networks of weakly coupled oscillators. *Nonlinearity* **1994**, *7*, 1623.
16. Flach, S.; Gorbach, A.V. Discrete breathers—Advances in theory and applications. *Phys. Rep.* **2008**, *467*, 1–116.
17. Rumpf, B. Simple statistical explanation for the localization of energy in nonlinear lattices with two conserved quantities. *Phys. Rev. E* **2004**, *69*, 016618.
18. Rumpf, B. Transition behavior of the discrete nonlinear Schrödinger equation. *Phys. Rev. E* **2008**, *77*, 036606.
19. Rumpf, B. Stable and metastable states and the formation and destruction of breathers in the discrete nonlinear Schrödinger equation. *Phys. D Nonlinear Phenom.* **2009**, *238*, 2067–2077.
20. Rumpf, B. Growth and erosion of a discrete breather interacting with Rayleigh-Jeans distributed phonons. *Europhys. Lett.* **2007**, *78*, 26001.
21. Iubini, S.; Franzosi, R.; Livi, R.; Oppo, G.; Politi, A. Discrete breathers and negative-temperature states. *New J. Phys.* **2013**, *15*, 023032.
22. Livi, R.; Franzosi, R.; Oppo, G.L. Self-localization of Bose-Einstein condensates in optical lattices via boundary dissipation. *Phys. Rev. Lett.* **2006**, *97*, 60401.
23. Franzosi, R.; Livi, R.; Oppo, G.L. Probing the dynamics of Bose–Einstein condensates via boundary dissipation. *J. Phys. B At. Mol. Opt. Phys.* **2007**, *40*, 1195.
24. Tsironis, G.; Aubry, S. Slow relaxation phenomena induced by breathers in nonlinear lattices. *Phys. Rev. Lett.* **1996**, *77*, 5225.
25. Piazza, F.; Lepri, S.; Livi, R. Slow energy relaxation and localization in 1D lattices. *J. Phys. A Math. Gen.* **2001**, *34*, 9803.
26. Piazza, F.; Lepri, S.; Livi, R. Cooling nonlinear lattices toward energy localization. *Chaos* **2003**, *13*, 637–645.

27. Reigada, R.; Sarmiento, A.; Lindenberg, K. Breathers and thermal relaxation in Fermi–Pasta–Ulam arrays. *Chaos* **2003**, *13*, 646–656.
28. De Roeck, W.; Huveneers, F. Asymptotic localization of energy in nondisordered oscillator chains. *Commun. Pure Appl. Math.* **2015**, *68*, 1532–1568.
29. Cuneo, N.; Eckmann, J.P. Non-equilibrium steady states for chains of four rotors. *Commun. Math. Phys.* **2016**, *345*, 185–221.
30. Oikonomou, T.; Nergis, A.; Lazarides, N.; Tsironis, G. Stochastic metastability by spontaneous localisation. *Chaos Solitons Fractals* **2014**, *69*, 228–232.
31. Geniet, F.; Leon, J. Energy transmission in the forbidden band gap of a nonlinear chain. *Phys. Rev. Lett.* **2002**, *89*, 134102.
32. Maniadis, P.; Kopidakis, G.; Aubry, S. Energy dissipation threshold and self-induced transparency in systems with discrete breathers. *Phys. D Nonlinear Phenom.* **2006**, *216*, 121–135.
33. Johansson, M.; Kopidakis, G.; Lepri, S.; Aubry, S. Transmission thresholds in time-periodically driven nonlinear disordered systems. *Europhys. Lett.* **2009**, *86*, 10009.
34. Iubini, S.; Lepri, S.; Livi, R.; Politi, A. Off-equilibrium Langevin dynamics of the discrete nonlinear Schroedinger chain. *J. Stat. Mech Theory Exp.* **2013**, *2013*, P08017 .
35. Borlenghi, S.; Iubini, S.; Lepri, S.; Chico, J.; Bergqvist, L.; Delin, A.; Fransson, J. Energy and magnetization transport in nonequilibrium macrospin systems. *Phys. Rev. E* **2015**, *92*, 012116.
36. Kulkarni, M.; Huse, D.A.; Spohn, H. Fluctuating hydrodynamics for a discrete Gross-Pitaevskii equation: Mapping onto the Kardar-Parisi-Zhang universality class. *Phys. Rev. A* **2015**, *92*, 043612.
37. Mendl, C.B.; Spohn, H. Low temperature dynamics of the one-dimensional discrete nonlinear Schroedinger equation. *J. Stat. Mech Theory Exp.* **2015**, *2015*, P08028.
38. Yoshida, H. Construction of higher order symplectic integrators. *Phys. Lett. A* **1990**, *150*, 262–268.
39. Rugh, H.H. Dynamical approach to temperature. *Phys. Rev. Lett.* **1997**, *78*, 772.
40. Iacobucci, A.; Legoll, F.; Olla, S.; Stoltz, G. Negative thermal conductivity of chains of rotors with mechanical forcing. *Phys. Rev. E* **2011**, *84*, 061108.
41. Ke, P.; Zheng, Z.G. Dynamics of rotator chain with dissipative boundary. *Front. Phys.* **2014**, *9*, 511–518.
42. Iubini, S.; Lepri, S.; Livi, R.; Politi, A. Boundary-induced instabilities in coupled oscillators. *Phys. Rev. Lett.* **2014**, *112*, 134101.
43. Iubini, S.; Lepri, S.; Livi, R.; Politi, A. Coupled transport in rotor models. *New J. Phys.* **2016**, *18*, 083023.
44. Ng, G.; Hennig, H.; Fleischmann, R.; Kottos, T.; Geisel, T. Avalanches of Bose–Einstein condensates in leaking optical lattices. *New J. Phys.* **2009**, *11*, 073045.
45. Eleftheriou, M.; Lepri, S.; Livi, R.; Piazza, F. Stretched-exponential relaxation in arrays of coupled rotators. *Phys. D Nonlinear Phenom.* **2005**, *204*, 230–239.